Rime- and glaze-ice accretion due to freezing rain falling vertically on a horizontal thermally insulated overhead line conductor

G. Poots and P. L. I. Skelton
Centre for Industrial Applied Mathematics, University of Hull, Hull, UK

A theory of atmospheric icing due to freezing rain on an overhead line conductor (OHLC) is developed. The rain falls vertically on a horizontal OHLC that is thermally insulated. It is assumed that the collection efficiency of the accretion surface is unity and that this surface is in thermodynamic equilibrium with the environment.

For air temperature $T_A \leqslant 0°C$ and raindrop temperature $T_D < 0°C$, the freezing rain accretes as rime ice, provided that the temperature of the ice surface $T_I < 0°C$. The evolution equation governing the mass transfer at the accretion surface is solved analytically, yielding the shape of the rime-ice surface. Equations governing the thermal state of the rime-ice deposit are also given. These determine the onset of wet growth or glaze accretion at the upper stagnation line during suitable environmental conditions.

For environmental conditions producing an ice surface at temperature $T_I = 0°C$, the freezing accretes as glaze. Equations governing the heat and mass transfer at the surface determine the shape of the glaze surface and the downward viscous motion of the unfrozen water. For $T_D < 0°C$, glaze evolution equations are developed for $T_A \leqslant 0°C$ and $T_A > 0°C$. Analytical solutions of these equations are obtained. In particular, when $T_D < -T_A < 0°C$, the evolution equation predicts a novel limiting growth that is triangular in shape. Further study of the mass and heat transfer conditions, in the neighborhood of this final stage of glaze accretion, shows that it is maintained in thermodynamic equilibrium with its warm air environment.

Keywords: overhead power conductors; freezing rain

Introduction

Atmospheric icing on an overhead line conductor (OHLC) due to freezing fog, freezing rain, and wet-snow accretion can cause two main types of problems, namely, increased quasi-steady loads from ice weight and wind load, and a windward instability of the conductor, known as galloping. Consequently, for design purposes, a major aim is to predict the intensity of ice loading and its evolutionary shape as a function of the mechanical and thermal properties of the OHLC, the wind speed and temperature, and basic meteorological data, all of which determine the mode of ice accretion during a period of time. A dynamical model that simulates rime-ice accretion due to freezing fog droplets on an OHLC of finite span and finite torsional stiffness has been constructed by Skelton and Poots (1990). Here it was assumed that droplets freeze on impaction. On the other hand, if droplets are slightly supercooled, only a fraction will usually freeze so that glaze icing occurs and the icing surface is covered by a liquid film. Mathematical models for the transition from rime to glaze icing on a fixed OHLC are developed in Poots and Skelton (1991a, 1991b). These models are based on the heat and mass transfer conditions at the accretion surface and its interaction with the environment. They entail the numerical solution of (two-dimensional (2-D)) dual moving-boundary problems and have provided results on the intensity of icing due to both freezing fog and freezing rain, as a function of the environmental temperature, wind speed, precipitation rate, and thermal properties of the OHLC.

The basic equations governing the equilibrium temperature of a thermally insulated surface in a variety of icing conditions, caused by the impaction of supercooled droplets, were first formulated and applied to an aerofoil by Messinger (1953). Later these equations were applied to the icing of a thermally insulated cylinder in a cross flow by Lozowski et al. (1983); see also the ice-accretion studies of Szilder et al. (1987) and Gent (1988).

A related area of study is concerned with icing by freezing rain that is falling vertically on elements of a grid system, such as on the towers, OHLCs, and stay lines. Here a theory is developed for such an accretion process occurring on a horizontal OHLC, and exact analytical solutions are derived. It is based on the following assumptions:

(1) supercooled raindrops fall vertically with terminal speed on a horizontal OHLC;
(2) for a specified rainfall precipitation rate $\mathscr{P}(\mathrm{mm}(H_2O)h^{-1})$, an average-sized raindrop, deduced from the Best (1950) spectrum of droplet size, is employed;

Address reprint requests to Dr. Poots at Centre for Industrial Applied Mathematics, University of Hull, Hull HU6 7RX, UK.

Received 14 November 1991; accepted 4 February 1992

Table 1 Raindrop parameters as a function of the precipitation rate $\mathscr{P}$ ($mm(H_2O)h^{-1}$)

$\mathscr{P}$ ($mm(H_2O)h^{-1}$)	G $g\cdot m^{-3}$	$\bar{r}_D$ (mm)	W ($m\cdot s^{-1}$)
0.5	0.04	0.49	3.7
1.0	0.07	0.58	4.3
1.5	0.09	0.63	4.6
2.0	0.12	0.68	4.9
4.0	0.22	0.79	5.5
6.0	0.31	0.87	5.8

(3) the collection efficiency of the horizontal OHLC, for an average-sized raindrop falling vertically, is unity;
(4) the surface of the OHLC is thermally insulated;
(5) during the accretion process, the free-convection heat transfer coefficient, h ($W\cdot m^{-2}K^{-1}$), for the ice surface is taken to be uniform and constant;
(6) during glaze accretion the effects of momentum exchange of impacting droplets on the motion of the unfrozen water, and the conversion of kinetic energy of impacting droplets into heat, are ignored;
(7) the physical properties of rime and glaze ice are constant and independent of the temperature.

For a given precipitation $\mathscr{P}(mm(H_2O)h^{-1})$, it is a simple matter to deduce, from Best (1950), the average-sized raindrop, of radius $\bar{r}_D(mm)$, and the equivalent liquid water content per unit volume of air, $G(kg\cdot m^{-3})$. The corresponding droplet terminal speed $W(m\cdot s^{-1})$ is available from Gunn and Kinzer (1949). In Tables 1 and 2, environmental and physical properties of the iced OHLC system are given for convenience.

The above assumptions now provide the basis for the construction of evolution equations governing the growth of rime- and glaze-ice accretion due to freezing rain falling vertically on a horizontal OHLC.

Rime accretion due to freezing rain

In the following, the suffixes I, W, and A are used to denote variables and properties of ice, water, and air, respectively. The radius of the conductor is denoted by $r_c(m)$. Cartesian coordinates (x, y), with origin at the center of the conductor, are employed in the construction of the mathematical model (see Figure 1). Let $\mathbf{j}$ be the unit vector in the y-direction, which is taken vertically upwards. Above the conductor an average-sized raindrop moves with terminal velocity

$$\mathbf{v}_T^* = -W\mathbf{j} \tag{1}$$

The axial growth of the rime-ice accretion surface in the vertical direction is denoted by

$$C = C(x, y, t) = 0 \tag{2}$$

The normal velocity at any point on the ice surface is given by $-\partial C/\partial t(\nabla C/|\nabla C|^2)$. It follows that, if E measures the distance along the normal trajectory to the growing ice-accretion surface, then

$$\partial E/\partial t = -(1/|\nabla C|)\partial C/\partial t \tag{3}$$

For rime-ice accretion, the ice surface temperature is always less than the fusion temperature, $T_F = 0°C$. Supercooled droplets at temperature $T_D \in [T_A, T_F]$ upon impaction with the ice surface, extract heat from the system to warm up to T_F, solidify and thereby release latent heat of fusion, adhere to the surface, and release further heat on cooling down to the temperature of the ice surface. The ice deposit loses heat at the surface by free convection, sublimation, and radiation. However, even though the conductor is thermally insulated, it is necessary to account for heat transfer within the ice by transient conduction. The latter was omitted in the earlier investigation of Lozowski et al. (1983).

For points on the accretion surface, within the window of

Notation

c	Specific heat, $J\cdot kg^{-1}\cdot K^{-1}$
C	Ice-accretion surface
E	Glaze-ice thickness, m
$e(T)$	Saturation vapor pressure, kPa
G	Liquid water content per unit volume of air, $kg\cdot m^{-3}$
h	Heat transfer coefficient, $W\cdot m^{-2}\cdot K^{-1}$
H	Atmospheric pressure, $k\cdot Pa$
$\mathbf{j}$	Unit vector in y-direction
k	Thermal diffusivity, $m^2\,s^{-1}$
K	Thermal conductivity, $W\cdot m^{-1}\cdot K^{-1}$
L	Latent heat, $J\cdot kg^{-1}$
M	Mass of ice loading per unit length of conductor, kg
$\mathbf{n}$	Unit normal vector on ice surface
Nu	Nusselt number
$\mathscr{P}$	Precipitation rate, $mm(H_2O)h^{-1}$
Pr	Prandtl number
r_c	Radius of conductor, m
r_D	Radius of droplet, mm
Ra	Rayleigh number
t	Time, s
T	Temperature, °C
$\tilde{\mathbf{v}} = (\tilde{u}, \tilde{v})$	Velocity of unfrozen water, $m\cdot s^{-1}$
$\mathbf{V}_T^*$	Terminal velocity of droplet, $m\cdot s^{-1}$
W	Terminal speed of average-sized droplet, $m\cdot s^{-1}$
(x, y)	Cartesian coordinates, m
$(\tilde{x}, \tilde{y})$	Intrinsic coordinates on conductor surface, m

Greek symbols

β	Volumetric thermal expansion coefficient, K^{-1}
γ	Heat transfer parameter
Δ	Thickness of unfrozen water layer, m
ε	Emissivity
ν	Kinematic viscosity, $m^2\cdot s^{-1}$
ρ	Density, $kg\cdot m^{-3}$
σ	Stefan–Boltzman constant, $W\cdot m^{-2}K^{-4}$
τ	Dimensionless time
ϕ	Angle
χ	Heat transfer parameter

Subscripts

A	Air
D	Droplet
E	Evaporation
F	Fusion
I	Ice
S	Sublimation
W	Water

Table 2 Physical properties of the OHLC icing system

		Ice	Water	Air
Density	ρ, kg·m^{-3}	917	1000	1.28
Specific heat	c, J·kg^{-1}K^{-1}	2040	4217	1006
Emissivity	ε	0.95		
Thermal conductivity	K, W·m^{-1}K^{-1}			2.42×10^{-2}
Kinematic viscosity	ν, m^2·s^{-1}			1.345×10^{-5}
Water content of air	G, kg·m^{-3}			0.05–0.29×10^{-3}
Latent heat of fusion	L_F, J·kg^{-1}		3.25×10^5	
Latent heat of evaporation	L_E, J·kg^{-1}		2.51×10^6	
Latent heat of sublimation	L_S, J·kg^{-1}		2.835×10^6	
Radius of OHLC	r_c, m		1.863×10^{-2}	

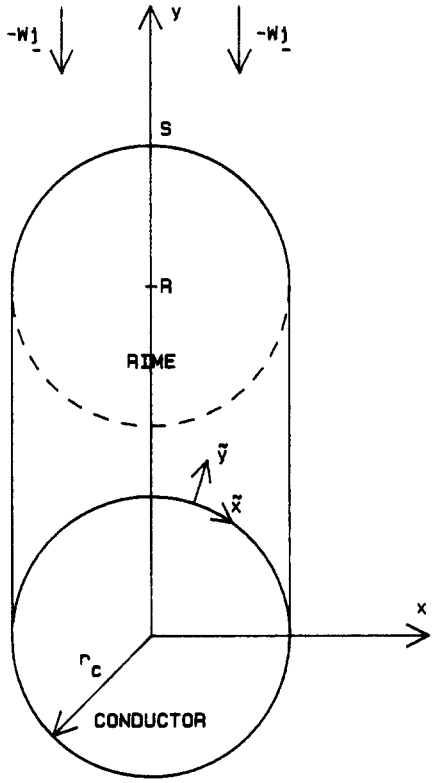

Figure 1 Schematic diagram of rime-iced OHLC: $R\left(0, \frac{GWt}{\rho_I}\right)$, $S\left(0, \frac{GWt}{\rho_I} + r_c\right)$

accretion $|x| < r_c$, $y > 0$, the mass transfer balance is

$$-\rho_I \frac{1}{|\nabla C|}\frac{\partial C}{\partial t} = GW\mathbf{j}\cdot\mathbf{n} \tag{4}$$

where $\mathbf{n} = \nabla C/|\nabla C|$ is chosen as the outward normal to the rime-ice surface $C = 0$ and ρ_I denotes the density of ice.

The heat transfer balance at the accretion surface accounting for heat conduction into the rime ice (see Poots and Skelton 1991a), is

$$GW[-c_W(T_F - T_D) + L_F + c_I(T_F - T_I)]\mathbf{j}\cdot\mathbf{n} - h(T_I - T_A) - \chi_S[e(T_I) - e(T_A)] - \sigma\varepsilon_I(T_I^4 - T_A^4) - K_I\nabla T_I\cdot\mathbf{n} = 0 \tag{5}$$

Here c, L, h, e, σ, ε, and K denote specific heat, latent heat, free-convection heat transfer coefficient, saturation vapor pressure, Stefan–Boltzman constant, emissivity, and thermal conductivity, respectively.

A polynomial approximation for calculating the saturation pressure $e(T)$ (kPa, over ice or over water) is available in Lowe (1977). Moreover, the heat and mass transfer analogy of Chilton and Colburn (1934) yields

$$\chi_S = 0.622hL_S/(c_A H_0 l^{2/3}) \tag{6}$$

where L_S is the latent heat of sublimation, H_0(kPa) is the total pressure of the ambient air, and $l = 0.875$ is the Lewis number.

The thermal transients within the rime ice are governed by

$$\rho_I c_I(\partial^2 T_I/\partial x^2 + \partial^2 T_I/\partial y^2) = K_I \partial T_I/\partial t \tag{7}$$

subject to the boundary condition (Equation 5) for the accretion surface, and the condition

$$\nabla T_I\cdot\hat{\mathbf{f}} = 0 \tag{8}$$

at the ice/conductor interface; here $\hat{\mathbf{f}}$ is the outward unit normal to the surface of the conductor.

To complete Equations 5 and 6, the free-convection heat transfer coefficient h must be specified. To date, experimental information on such heat transfer coefficients, for evolving ice surfaces, are not available. Consequently, as in Lozowski et al. (1983) and Poots and Skelton (1991a, 1991b), empirical correlations for uniced circular cylinders are adopted. For example, h may be replaced by an average value

$$\bar{h} = \overline{\mathrm{Nu}}K_A/2r_c \tag{9}$$

where $\overline{\mathrm{Nu}}$ is the average free-convection Nusselt number for a circular cylinder. For nonicing conditions, a relevant correlation given by Churchill and Chu (1975) for the Rayleigh-number range $\mathrm{Ra_D} \in [10^{-5}, 10^{12}]$ is

$$\overline{\mathrm{Nu}} = \left\{0.60 + \frac{0.387\mathrm{Ra_D^{1/6}}}{[1 + (0.559/\mathrm{Pr})^{9/16}]^{8/27}}\right\}^2 \tag{10}$$

The Rayleigh number is

$$\mathrm{Ra_D} = g\beta_A(T_I - T_A)(2r_c)^3\mathrm{Pr}_A/\nu_A^2 \tag{11}$$

where the Prandtl number $\mathrm{Pr} = \nu/k$. Here $\beta = -\frac{1}{\rho}\left(\frac{\partial\rho}{\partial T}\right)_{H_0}$ is the volumetric thermal expansion coefficient, g the gravitational constant, ν the kinematic viscosity, and k the thermal diffusivity; note that all properties are evaluated at the film temperature $T_f = (T_I + T_A)/2$ and, moreover, T_I is to be introduced as an average ice surface temperature.

For rime-ice accretion, the mass transfer balance (Equation 4) is the evolution equation for the accretion surface. Introducing the following dimensionless variables

$$X = x/r_c, \quad Y = y/r_c, \quad T = (GWt)/(\rho_I r_c) \tag{12}$$

Equation 4 simply becomes

$$\frac{\partial C}{\partial T} = -\mathbf{j}\cdot\nabla C = -\frac{\partial C}{\partial Y} \tag{13}$$

where the operator $\nabla = (\partial/\partial X, \partial/\partial Y)$. The required solution for $T > 0$ is

$$\left.\begin{aligned} C &= X^2 + (Y-T)^2 - 1 = 0, \quad Y > T, \quad |X| \in [0,1] \\ C &= |X| - 1 = 0, \quad Y \in [0,T], \quad |X| \in [0,1] \end{aligned}\right\} \tag{14}$$

In physical terms, this semicircular front (see Figure 1) has radius r_c with center at $(0, GWt/\rho_I)$. This is, of course, the large relaxation time approximation (LRTA) for the problem of rime-ice accretion on a conductor in a cross flow of velocity W (see Poots and Rodgers 1976). Indeed, it is the inertia of raindrops falling at terminal speed that justifies the use of Assumption 3 above, so that together Assumptions 1 and 3 are equivalent to the LRTA for vertical freezing rain. For a 1 m length of OHLC, the mass of ice deposited is given by

$$M(t)/\rho_I r_c^2 = 2T = \frac{2GWt}{\rho_I r_c} \tag{15}$$

The applicability of this simple solution (Equations 14 and 15) depends on the thermal state of the rime deposit, as governed by Equations 5 to 11. During rime-ice accretion the temperature of the ice deposit is less than 0°C. The hottest part of the deposit will be at the upper stagnation line $S(0, r_c + GWt/\rho_I)$; at the conductor shoulder $(r_c, 0)$, the ice temperature will be T_A. However, when T_A is just below 0°C, the temperature of the rime-ice surface in the vicinity of the stagnation line S may rise to 0°C. When this occurs, wet growth or glaze accretion spreads downwards, enveloping the underlying rime growth determined by Equation 14.

The solution of the (nonlinear) dual moving-boundary problems, which control this transition from rime to glaze, must be obtained by numerical methods as described in Poots and Skelton (1991a, 1991b). This aspect of the freezing-rain problem will not be considered further, for in practice, since the OHLC is thermally insulated, it is likely that the onset of glaze in air temperatures just below 0°C will occur almost instantaneously.

Wet growth due to freezing rain

Wet growth or glaze ice occurs when the mass rate of impaction of supercooled raindrops is greater than the mass rate of freezing. Since water and ice coexist at the fusion temperature, and the OHLC is thermally insulated, it follows that the glaze-ice deposit and the unfrozen water flowing downwards from the upper stagnation line are at the fusion temperature.

For convenience (see Figure 1) let $\tilde{x}$ and $\tilde{y}$ be intrinsic coordinates attached to the conductor surface ($\tilde{x} = r_c(\pi - \theta)$, $\tilde{y} = r - r_c$, where (r, θ) are polar coordinates). In the control volume on the conductor surface at $(\tilde{x}, \tilde{x} + \delta\tilde{x})$, as shown schematically in Figure 2, let the glaze-ice thickness be $E(\tilde{x}, t)$ and $\tilde{\mathbf{v}} = (\tilde{u}, \tilde{v})$ be the velocity field in the downward flow of the unfrozen water within the thin layer of thickness $\Delta(\tilde{x}, t)$.

The mass transfer balance for the glaze accretion and the flow of unfrozen water out of and into the control volume (see Poots and Skelton 1991b) yields

$$\rho_I \frac{\partial E}{\partial t} + \rho_W \frac{\partial}{\partial \tilde{x}} \int_E^{E+\Delta} \tilde{u}\, d\tilde{y} = GW\mathbf{j}\cdot\mathbf{n} \tag{16}$$

On impaction, the supercooled raindrops extract heat from the glaze surface to warm up to the fusion temperature. Part of this mass impingement, as determined by Equation 16, will solidify releasing latent heat, and the remainder participates in the flow and heat transfer of the unfrozen water from face $(\tilde{x})$ to $(\tilde{x} + \delta\tilde{x})$. Globally the glaze surface either loses or gains heat from the environment, depending on whether the air temperature is less or greater than the fusion temperature.

The different glaze growth modes associated with $T_A < T_F$, $T_A = T_F$, and $T_A > T_F$ are now examined.

Glaze accretion for $T_A < T_F$

The glaze accretion surface loses heat to the environment by free convection, evaporation, and radiation. Consequently the heat balance for the control volume (see Poots and Skelton 1991b) is

$$\begin{aligned} &-GWc_W(T_F + T_D)\mathbf{j}\cdot\mathbf{n} + \rho_I L_F \frac{\partial E}{\partial t} \\ &-\frac{\partial}{\partial \tilde{x}} \int_E^{E+\Delta} \rho_W c_W (T_F - T_A)\tilde{u}\, d\tilde{y} - \bar{h}(T_F - T_A) \\ &-\chi_E[e(T_F) - e(T_A)] - \sigma\varepsilon(T_F^4 - T_A^4) = 0 \end{aligned} \tag{17}$$

The heat and mass transfer analogy of Chilton and Colburn (1934) yields

$$\chi_E = 0.622\bar{h}L_E/(c_A H_0 l^{2/3}) \tag{18}$$

where L_E is the latent heat of evaporation. The average heat transfer coefficient $\bar{h}$ is given by Equations 9 and 10 at Rayleigh number

$$\mathrm{Ra}_D = g\beta_A(T_F - T_A)(2r_c)^3\,\mathrm{Pr}_A/\nu_A^2 \tag{19}$$

and all properties are evaluated at the film temperature $T_f = (T_F + T_A)/2$.

Clearly, on using Equation 16, the term involving the convective heat transfer of the unfrozen water in Equation 17

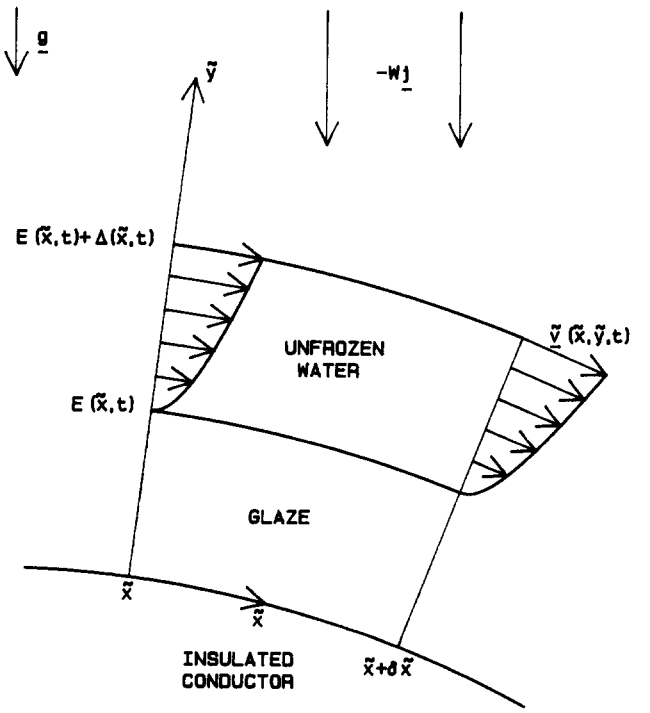

Figure 2 Schematic diagram of glaze accretion and flow of unfrozen water

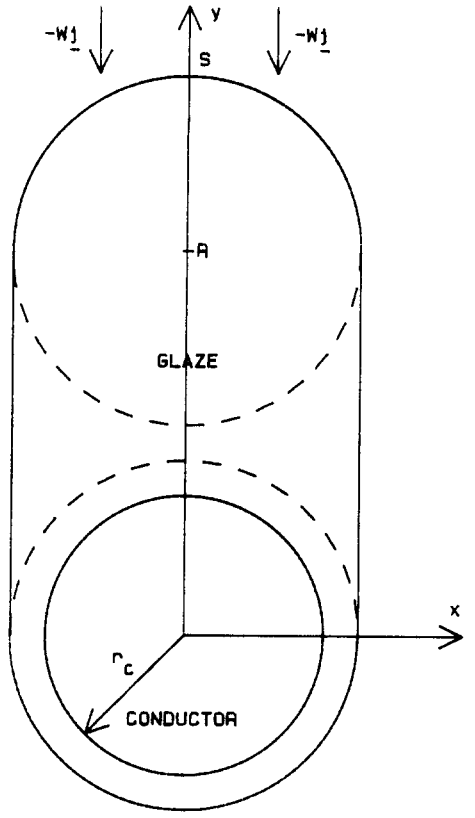

Figure 3 Schematic diagram of glaze-iced OHLC for $T_A < 0°C$: $R(0, \gamma\tau r_c)$, $S(0, (1 + (\gamma + 1)\tau)r_c)$

can be eliminated to give the glaze evolution equation

$$-\rho_I[L_F + c_W(T_F - T_A)]\frac{\partial C}{\partial t}\frac{1}{|\nabla C|} = c_W(2T_F - T_D - T_A)GW\mathbf{j}\cdot\mathbf{n} + \bar{h}(T_F - T_A) + \chi_E[e(T_F) - e(T_A)] + \sigma\varepsilon(T_F^4 - T_A^4) \quad (20)$$

For raindrops slightly supercooled below fusion temperature, it is sufficient to write

$$e(T_F) - e(T_A) = (T_F - T_A)(\partial e/\partial T)_{T_F} \quad (21)$$

where $(\partial e/\partial T)_{T_F} = 0.04438$ (kPa/°C) (see Lowe 1977). To the same level of approximation, the radiation term in Equation 17 is simplified on assuming

$$T_F^4 - T_A^4 = (T_F - T_A)(4T_F^3) \quad (22)$$

Consequently, on introducing the modified heat transfer coefficient

$$h^* = \bar{h}[1 + \{0.622L_E(\partial e/\partial T)_{T_F}/c_A H_0 l^{2/3}\}] + 4\sigma\varepsilon T_F^3 \quad (23)$$

the dimensionless heat transfer ratio

$$\gamma = \frac{GWc_W}{h^*}\frac{(2T_F - T_D - T_A)}{|T_F - T_A|} \quad (24)$$

and the dimensionless variables

$$X = x/r_c, \qquad Y = y/r_c, \qquad \tau = \frac{h^*|T_F - T_A|}{\rho_I[L_F + c_W(T_F - T_A)]}\frac{t}{r_c} \quad (25)$$

the glaze solution equation 20 simplifies to

$$-\frac{\partial C}{\partial \tau} = \gamma\mathbf{j}\cdot\nabla C + |\nabla C| = \gamma\mathbf{j}\cdot\nabla C + \mathrm{sgn}(T_F - T_A)|\nabla C| \quad (26)$$

For those parts of the glaze/OHLC system lying outside the window of accretion, where raindrops cannot impact, the evolution equation reduces to

$$-\frac{\partial C}{\partial \tau} = |\nabla C| \quad (27)$$

This is equivalent to setting $W = 0$, giving $\gamma = 0$.

Although the evolution equations 26 and 27 are nonlinear, they can be solved analytically. The required solution (see Figure 3) is

$$C = X^2 + (Y - \gamma\tau)^2 - (1 + \tau)^2 = 0, \quad Y \in [\gamma\tau, 1 + (\gamma + 1)\tau], \quad |X| \in [0, 1 + \tau] \quad (28)$$

$$C = |X| - (1 + \tau) = 0, \quad Y \in [0, \gamma\tau] \quad (29)$$

and

$$C = X^2 + Y^2 - (1 + \tau)^2 = 0, \quad Y \in [-1 - \tau, 0], \quad |X| \in [0, 1 + \tau] \quad (30)$$

Thus, in contrast to rime-ice accretion, given by Equation 14, the nonlinear process of glaze accretion for $T_A < T_F$ exists on a long time scale; also, for glaze the window of accretion $|X| \in [0, 1 + \tau]$ is increasing with time and, moreover, the glaze ice completely surrounds the OHLC.

During the glaze accretion for $T_A < T_F$, the ice loading per unit length of conductor in freezing rain is given by

$$M/\rho_I r_c^2 = 2(\pi + \gamma)\tau + (\pi + 2\gamma)\tau^2 \quad (31)$$

Glaze accretion for $T_A = T_F$

For this mode of glaze accretion, there is no heat exchange with the environment, and the evolution equation 20 simplifies to

$$-\rho_I L_F\frac{\partial C}{\partial t}\frac{1}{|\nabla C|} = c_W(T_F - T_D)GW\mathbf{j}\cdot\mathbf{n} \quad (32)$$

In terms of the dimensionless variables

$$X = x/r_c, \qquad Y = y/r_c, \qquad \tilde{\tau} = \frac{c_W(T_F - T_D)GW}{\rho_I L_F r_c} \quad (33)$$

the glaze evolution equation 32 simplifies to

$$-\frac{\partial C}{\partial \tilde{\tau}} = \mathbf{j}\cdot\nabla C = \frac{\partial C}{\partial Y} \quad (34)$$

which has solution

$$C = X^2 + (Y - \tilde{\tau})^2 - 1 = 0, \quad Y \in [\tilde{\tau}, 1 + \tilde{\tau}], \quad |X| \in [0, 1] \quad (35)$$

In physical terms, this semicircular glaze front has radius r_c with center at $\left(0, \frac{c_W(T_F - T_D)GW}{\rho_I L_F}t\right)$. For $y < 0$ the conductor surface is free from glaze icing and, apart from the different time scale, this mode of glaze accretion is identical in shape to rime deposits occurring when $T_A \leqslant 0°C$ (see Equation 14).

During this mode of glaze growth, the ice loading per unit length of conductor in freezing rain is given by

$$M/\rho_I r_c^2 = 2\tilde{\tau} = 2\frac{c_W(T_F - T_D)GW}{\rho_I L_F r_c}t \quad (36)$$

Glaze accretion for $T_A > T_F$ ($0 < T_A < -T_D$)

The accretion surface now gains heat from the environment by free convection, condensation, and radiation. The heat balance

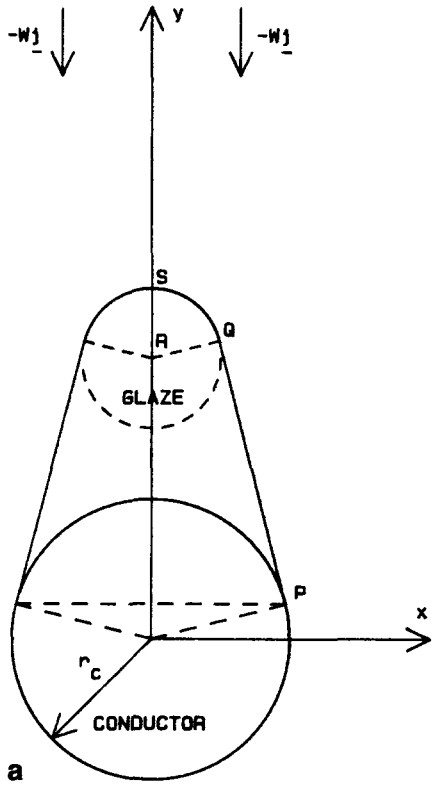

Figure 4(a) Schematic diagram of glaze-iced OHLC for $T_A > 0°C$: $P\left(\frac{(\gamma^2-1)^{1/2}}{\gamma}r_c, \frac{1}{\gamma}r_c\right)$, $Q\left[(1-\tau)\frac{(\gamma^2-1)^{1/2}}{\gamma}r_c, \left(\frac{1}{\gamma}(1-\tau)+\gamma\tau\right)r_c\right]$, $R(0, \gamma\tau r_c)$, $S(0, (1+(\gamma-1)\tau)r_c)$

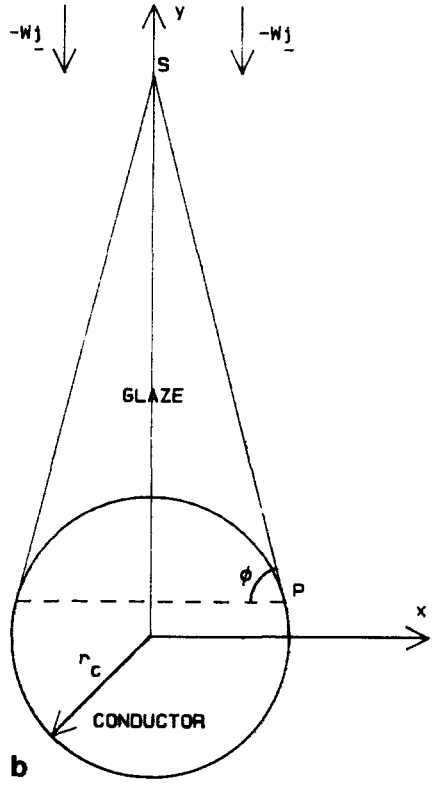

Figure 4(b) Schematic diagram of limiting glaze growth on an OHLC for $T_A > 0°C$: $P\left(\frac{(\gamma^2-1)^{1/2}}{\gamma}r_c, \frac{1}{\gamma}r_c\right)$, $S(0, \gamma r_c)$

for the control volume is given by Equation 20, namely,

$$-\rho_I[L_F + c_W(T_F - T_A)]\frac{\partial C}{\partial t}\frac{1}{|\nabla C|} = c_W(2T_F - T_D - T_A)GW\mathbf{j}\cdot\mathbf{n} - h^*(T_A - T_F) \quad (37)$$

where the modified heat transfer coefficient h^* is as defined in Equation 23. Inspection of Equation 37 shows that $|T_D| > T_A$ for glaze accretion to occur. Introducing γ, as defined in Equation 24, and the variables (Equations 25), the glaze evolution equation 37 simplifies to

$$-\frac{\partial C}{\partial \tau} = \gamma\mathbf{j}\cdot\nabla C - |\nabla C| = \gamma\mathbf{j}\cdot\nabla C + \mathrm{sgn}(T_F - T_A)|\nabla C| \quad (38)$$

The required solution (see Figures 4a and 4b) is

$$C = X^2 + (Y - \gamma\tau)^2 - (1-\tau)^2 = 0, \quad Y \in \left[\gamma\tau + \frac{1}{\gamma}(1-\tau), \gamma\tau + 1 - \tau\right] \quad (39)$$

$$C = Y - \gamma + (\gamma^2-1)^{1/2}|X| = 0, \quad Y \in \left[\frac{1}{\gamma}, \gamma\tau + \frac{1}{\gamma}(1-\tau)\right] \quad (40)$$

and

$$C = X^2 + Y^2 - 1 = 0, \quad Y \in \left[-1, \frac{1}{\gamma}\right] \quad (41)$$

It depicts a semicircular front of decreasing radius $r_c(1-\tau)$, with center at location $(0, \gamma\tau r_c)$. Two important features of this growth mode are

(1) glaze accretion cannot exist for values of the heat transfer parameter $\gamma < 1$;
(2) for $\gamma > 1$ the glaze loading ceases at $\tau = 1$, when the glaze growth limit is triangular in shape.

In connection with the glaze growth limit (see Figure 4b), the apex of the triangular deposit is $S(0, \gamma r_c)$. The sloping glaze face is tangential to the conductor at $P\left(\frac{(\gamma^2-1)^{1/2}}{\gamma}r_c, \frac{1}{\gamma}r_c\right)$. The angle of inclination of this face to the horizontal is given by

$$\phi = \tan^{-1}(\gamma^2-1)^{1/2} \quad (42)$$

Moreover, for $\gamma > 1$, in the growth time interval $\tau \in [0, 1]$, the ice loading per unit length of conductor is given by

$$M/\rho_I r_c^2 = \{(\gamma^2-1)^{1/2} - \phi\}(2\tau - \tau^2) \quad (43)$$

Consider now, in more detail, the structure of the glaze limit solution at $\tau = 1$. In particular, the mechanism for the maintenance of this limiting growth, in thermodynamic equilibrium with the environment for $\tau > 1$, should be explained. Clearly, at any point on the sloping face (Equation 40), the heat supplied by the environment is sufficient to warm the impacting droplets to the fusion temperature, and therefore no further ice is deposited. The unfrozen water flow bathes the limiting growth shape and the uniced part of the OHLC, and is now governed by the steady-state viscous flow in the water layer, which is driven by the gravitational buoyancy force. This aspect of the glaze process is not considered further, since it involves a simple application of the thin liquid film

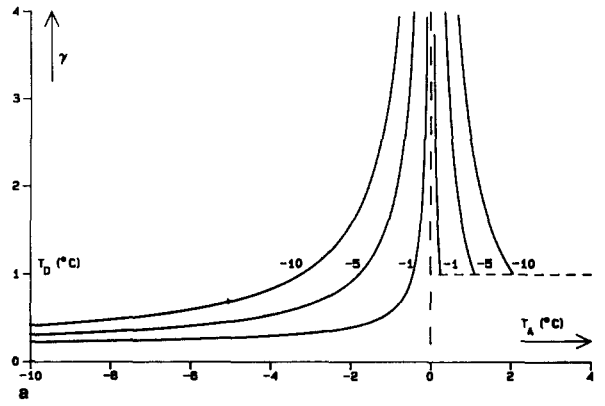

Figure 5(a) Glaze heat transfer parameter γ corresponding to a precipitation rate $\mathscr{P} = 2\text{mm}(H_2O)h^{-1}$, as a function of the air temperature T_A, at specified droplet temperature T_D

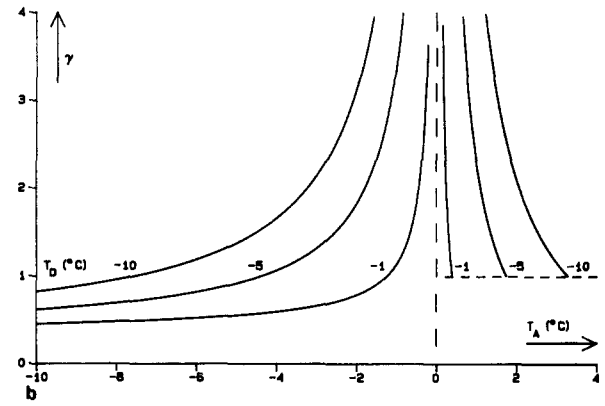

Figure 5(b) Glaze heat transfer parameter γ corresponding to a precipitation rate $\mathscr{P} = 4\text{mm}(H_2O)h^{-1}$, as a function of the air temperature T_A, at specified droplet temperatures T_D

approximation in conjunction with the surface mass transfer conditions

$$\rho_W \frac{\partial}{\partial \tilde{x}}\left(\int_E^{E+\Delta} \tilde{u}\, d\tilde{y}\right) = \begin{cases} GW\mathbf{j}\cdot\mathbf{n} & \text{for } Y \geqslant 0, \\ 0, & \text{for } Y < 0 \end{cases} \tag{44}$$

For details, see the time-dependent study of rime and glaze accretion by freezing rain on horizontal substrates given by Poots and Skelton (1992).

This completes the analysis for glaze accretion by freezing rain on a horizontal OHLC. The solutions of the governing nonlinear evolution equations, for $T_A \leqslant 0°$ and $T_A > 0°C$, are of considerable mathematical interest, since they are also exact solutions of 2-D nonlinear moving-boundary problems of the Stefan type. A novel feature of the analysis is the prediction of limiting triangular growth for $T_A > 0°C$, which is maintained by the prevailing environmental conditions. This growth mode is analogous to that observed in the flow of granular material when piled. The latter is characterized in terms of an angle of repose (see Sokolovskii 1965). In the same way, the limiting growth for glaze is characterized by the "thermal angle of repose" ϕ, as introduced by Equation 42.

Results on glaze accretion

Illustrative results are now given for glaze accretion due to freezing rain on an insulated OHLC of radius $r_c = 1.863 \times 10^{-2}$ m. In particular, the modes of glaze accretion at air temperatures, T_A, just below and above the fusion temperature $T_F = 0°C$ are highlighted. Figures 5 to 8 give results for the rainfall precipitation rate $\mathscr{P} = 2\text{mm}(H_2O)h^{-1}$, with corresponding water content $G = 0.12 \times 10^{-3}\,\text{kg}\cdot\text{m}^{-3}$ and terminal velocity $W = 4.9\,\text{m}\cdot\text{s}^{-1}$, and $\mathscr{P} = 4\text{mm}(H_2O)h^{-1}$ with $G = 0.22 \times 10^{-3}\,\text{kg}\cdot\text{m}^{-3}$ and $W = 5.5\,\text{mm}\cdot\text{s}^{-1}$.

In Figure 5a, the value of the dimensionless parameter γ is displayed as a function of the air temperature for $\mathscr{P} = 2\text{mm}(H_2O)h^{-1}$ at droplet temperatures $T_D = -1°C$, $-5°C$, and $-10°C$. For air temperature $T_A \in [-10, 0)°C$ the curves are continuous, with $\gamma \to GWc_W/h^*$ as $T_D \to 0^-$, and at the special case $T_A = 0°C$, γ is not defined. In this mode of accretion (see Figure 3), icing also occurs on the lower portion of the OHLC provided that $T_A < 0°C$. However, as previously described, when $T_A = 0°C$, glaze icing cannot exist on the lower portion of the OHLC, and the surface evolves as for rime ice, as displayed in Figure 1. For $T_A > 0°C$, γ must satisfy the condition $\gamma > 1$ for the existence of a solution and this cutoff is indicated in Figure 5a. Now the mode of accretion is as displayed in Figure 4a, leading to an associated limiting growth profile (see Figure 4b). The angle of inclination of this sloping ice surface to the horizontal, ϕ, is shown in Figure 6a for $T_A > 0°C$ and $T_D = -10(2) - 2°C$, when $\mathscr{P} = 2\text{mm}(H_2O)h^{-1}$. As $T_A \to 0^+$, $\gamma \to \infty$, and $\phi \to \pi/2$, thus approaching the mode of accretion at $T_A = 0°C$.

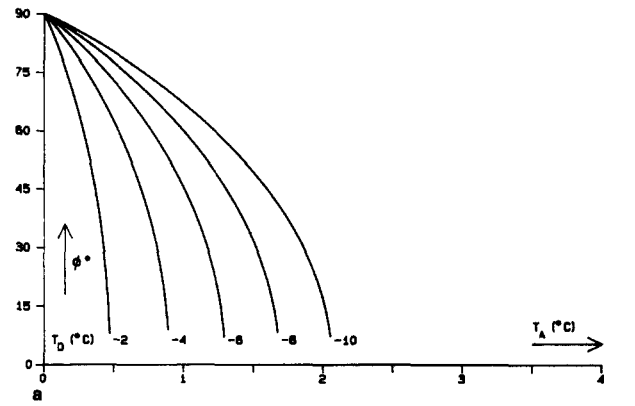

Figure 6(a) Angle ϕ for limiting glaze growth corresponding to a precipitation rate $\mathscr{P} = 2\text{mm}(H_2O)h^{-1}$, as a function of the air temperature T_A, at specified droplet temperatures T_D

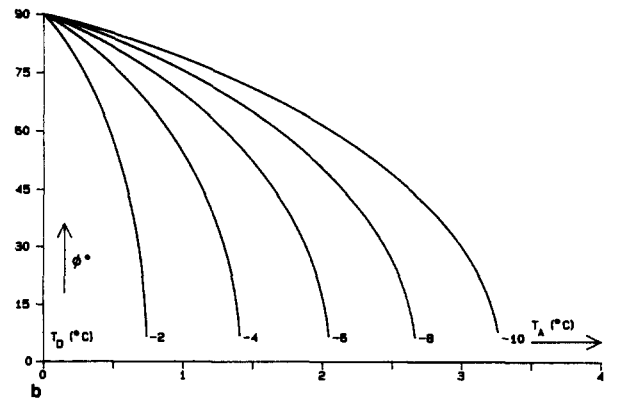

Figure 6(b) Angle ϕ for limiting glaze growth corresponding to a precipitation rate $\mathscr{P} = 4\text{mm}(H_2O)h^{-1}$, as a function of the air temperature T_A, and specified droplet temperatures T_D

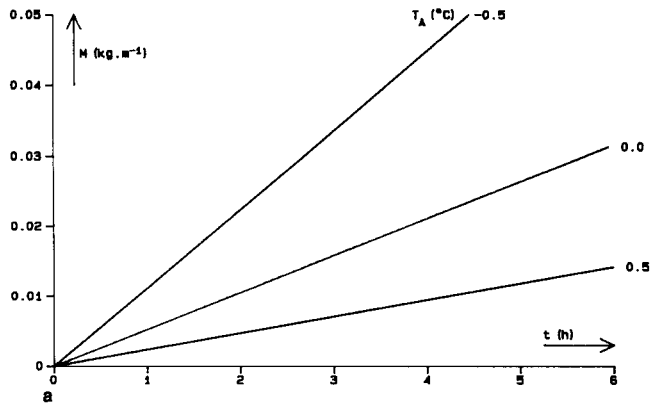

Figure 7(a) Glaze-ice loading $M(\mathrm{kg \cdot m^{-1}})$ as a function of the time for $T_D = -5°C$ and $T_A = -0.5, 0, 0.5°C$ for $\mathscr{P} = 2\mathrm{mm}(H_2O)h^{-1}$

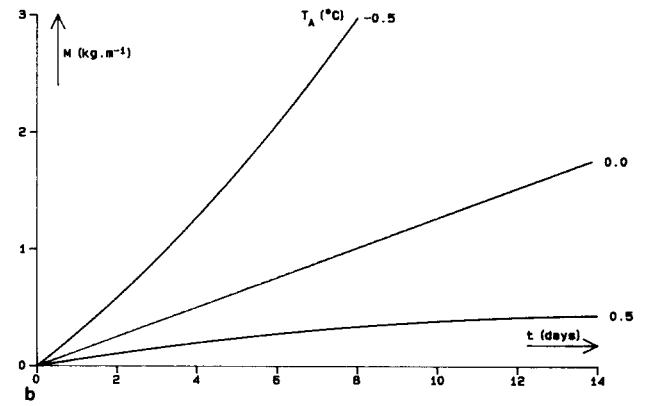

Figure 7(b) Glaze-ice loading $M(\mathrm{kg \cdot m^{-1}})$ in the long time period to form limiting growth for $T_D = -5°C$ and $T_A = -0.5, 0, 0.5°C$ for $\mathscr{P} = 2\mathrm{mm}(H_2O)h^{-1}$

Figures 5b and 6b show the corresponding results on increasing the precipitation rate to $\mathscr{P} = 4\mathrm{mm}(H_2O)h^{-1}$. Clearly, increasing $\mathscr{P}$ increases γ and hence ϕ.

Figure 7a provides a comparison of mass of ice accreted between the three cases $T_A < 0°C$, $T_A = 0°C$, and $T_A > 0°C$. The mass accreted at $T_A = 0°C$ provides a lower bound for that at $T_A < 0°C$ and an upper bound for that at $T_A > 0°C$, at any time $t > 0$. The results given here are for mass of ice per unit length at air temperatures $T_A = -0.5$, 0 and 0.5°C, with a droplet temperature of $T_D = -5°C$ and precipitation rate $\mathscr{P} = 2\mathrm{mm}(H_2O)h^{-1}$ when $r_c = 1.863 \times 10^{-2}$ m. Figure 7a gives the results for $t \in [0, 6]h$. Figure 7b covers the period $t \in [0, 14]$ days, after which time the glaze-accretion process in warm air attains its limiting growth and no further glaze ice is deposited. The latter is included so as to draw attention to the long time scales that may be encountered in studies of glaze evolution.

The limiting growth solutions, existing for $\tau > 1$, are displayed in Figure 8, for $T_D = -10°C$ and $\mathscr{P} = 2\mathrm{mm}(H_2O)h^{-1}$, at air temperatures $T_A = 1.25°C$, 1.50°C, and 1.75°C. Increasing precipitation rate or droplet temperature, or decreasing air temperature $T_A > 0°C$, increases the proportion of water that freezes to form the ice deposit, and hence the angle ϕ.

The above theory is based on an average heat transfer coefficient, for the natural convection updraft when $T_A < 0°C$ and for the downdraft when $T_A > 0°C$, calculated using empirical correlations of free convection on cylinders in

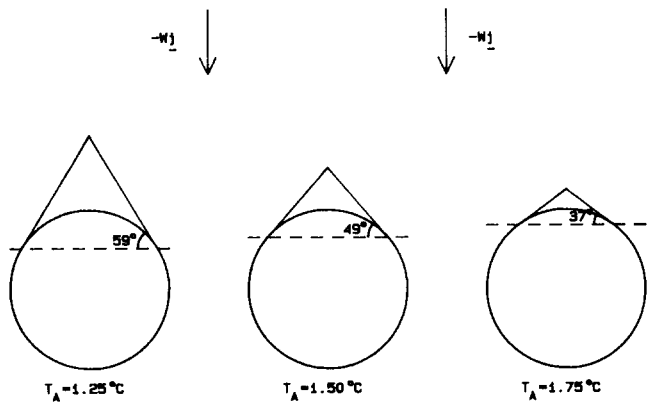

Figure 8 Limiting triangular growth shapes for various values of T_A when $T_D = -10°C$ and $\mathscr{P} = 2\mathrm{mm}(H_2O)h^{-1}$

nonicing conditions. In this connection it should be noted that for glaze icing on an OHLC in a crossflow (see Poots and Skelton 1991a, 1991b), the glaze accretion system is almost insensitive to the use of a variable heat transfer coefficient and even to data introduced to simulate ice surface roughness.

It is not possible at this stage to compare theoretical predictions of glaze accretion by freezing rain with those observed in field observations. However, an active program for the monitoring of natural ice accretions on OHLCs now exists in the UK environment (see Tunstall and Koutselos 1986; Eeles et al. 1988). It is hoped that the sensitivity of the above theory to the various assumptions that must be incorporated can ultimately be discussed when field data is available.

Conclusions

A theoretical study of ice accretion due to freezing rain falling vertically on a horizontal thermally insulated OHLC, which describes the heat and mass transfer mechanisms for rime and glaze accretion, is presented. In the case of glaze accretion, nonlinear evolution equations are derived, for which (exact) analytical results are obtained for the three different growth modes, depending on whether $T_A < 0°C$, $T_A = 0°C$, or $T_A > 0°C$. It is shown that the mass of ice accreted increases with decreasing air temperature, decreasing droplet temperature, or increasing rainfall precipitation rate. For positive air temperatures, a novel limiting glaze growth mode is predicted, which can exist in equilibrium with the environment. The formation of these triangular-shape limits for glaze is in contrast to the limiting-growth solutions for rime-ice axial growth, caused by the aerodynamic streamlining of the ice surface (see Skelton and Poots 1989).

Acknowledgments

The authors are indebted to National Grid R & D Centre (Leatherhead, UK) for providing a contract to undertake this investigation, which is published by permission of the National Grid Company.

References

Best, A. C. 1950. The size of raindrops. *Q.J.R. R. Met. Soc.*, **76**, 16–36

Chilton, T. J. and Colburn, A. P. 1934. Mass transfer coefficients. *Ind. Eng. Chem.*, **26**, 1183–1187

Churchill, S. W. and Chu, H. H. S. 1975. Correlating equations for laminar and turbulent free convection from a horizontal cylinder. *Int. J. Heat Mass Transfer*, **18**, 1049–1053

Eeles, W. T., Wareing, J. B., Strutt, I., Castle, D., and Amor, K. 1988. An automatic computer controlled weather actuated camera system for the investigation of snow accretion on overhead lines. *Proc. Fourth International Conference on Atmospheric Icing of Structures*, EDF Paris, 282–286

Gent, R. W. 1988. "HOV-ACC"—An aerofoil ice accretion prediction program for steady two-dimensional compressible flow conditions. RAE technical report 88052 Farnborough, UK

Gunn, R. and Kinzer, G. D. 1949. The terminal velocity of fall for water droplets in stagnant air. *J. Meteor.*, **6**, 243–248

Lowe, P. R. 1977. An approximating polynomial for the computation of saturation vapour pressure. *J. Appl. Meteor.*, **16**, 100–103

Lozowski, E. P., Stallabrass, J. R., and Hearty, P. F. 1983. The icing of an unheated, nonrotating cylinder. Part I: A simulation model. *J. Clim. Appl. Met.*, **22**, 2053–2062

Messinger, B. L. 1953. Equilibrium temperature of an unheated icing surface as a function of the air speed. *J. Aero. Sci.*, **20** (1), 29–42

Poots, G. and Rodgers, G. G. 1976. The icing of a cable. *J. Inst. Math. Appl.*, **18**, 203–217

Poots, G. and Skelton, P. L. I. 1991a. A time-dependent heat and mass transfer model for icing of overhead transmission lines: Rime ice and the onset of glaze. *Math. Eng. Ind.*, in press

Poots, G. and Skelton, P. L. I. 1991b. A time-dependent heat and mass transfer model for icing of overhead transmission lines: The transition from rime to glaze. *Math. Eng.*, in press

Poots, G. and Skelton, P. L. I. 1992. A simple mathematical model for rime and glaze accretion due to freezing rain on a horizontal plane surface. *Atmos. Environ.* **26**A(6), 1029–1040

Skelton, P. L. I. and Poots, G. 1989. The growth limits of rime-ice accretion on fixed conductors. *Mech. Res. Communic.*, **16** (4), 247–254

Skelton, P. L. I. and Poots, G. 1990. A dynamical model of rime-ice accretion on an overhead transmission line of finite torsional stiffness. *Math. Eng. Ind.*, **3** (1), 1–24

Sokolovskii, V. V. 1965. *Statics of Granular Media*. Pergammon, New York

Szilder, K., Lozowski, E. P., and Gates, E. M. 1987. Modelling ice accretion on non-rotating cylinders—the incorporation of time dependence and internal heat conduction. *Cold Regions Sci. Tech.*, **13**, 177–191

Tunstall, M. J. and Koutselos, L. 1986. Collection and reproduction of natural ice shapes on overhead line conductors and measurement of their aerodynamic characteristics. *Proc. Third International Conference on Atmospheric Icing of Structures*, Hydro, Vancouver, BC